

RESEARCH PAPER

Synthesis, Characterization, Structural, Optical and Photocatalyst Properties of C₆₀-ZnO-TiO₂ Nano Hybrid

Wasan M. Mohamed, Zainab SH. Mohammed, Mulamahawsh Anfal Fadhil *

College of Science for Women, Laser Physics Department, University of Babylon, Babylon, Iraq

ARTICLE INFO

Article History:

Received 04 October 2023

Accepted 23 December 2023

Published 01 January 2024

Keywords:

Fullerene

Nanocomposites

Photocatalyst

Sol-gel method

ABSTRACT

C₆₀-TiO₂-ZnO, C₆₀-ZnO, C₆₀-TiO₂ nanocomposites were synthesized using sol-gel method. Structural, chemical, and optical properties of nanocomposites were characterized using X-ray diffraction (XRD), tunneling electron microscopy (TEM), Fourier transform infrared (FTIR) spectroscopy, and photoluminescence (PL) spectroscopy. In addition to the fullerene peak, structural results in C₆₀-ZnO samples show the wurtzite hexagonal structure of zinc oxide. The peaks related to both anatase and rutile phases are observed in the sample of C₆₀-TiO₂ composite. All peaks related to fullerene (C), wurtzite phase of zinc oxide (W) and anatase (A) and rutile (R) phases of titanium dioxide are also exactly the same as C₆₀-ZnO and C₆₀-TiO₂ single composites in XRD analysis results of C₆₀-TiO₂-ZnO nanocomposites. The results of TEM images show that fullerene nanoparticles are located outside the surface of the zinc oxide and titanium dioxide nanoparticles. Titanium nanoparticles is less than 30nm and zinc oxide nanoparticles is less than 50nm in size. The photoluminescence (PL) spectrum measured for C₆₀-TiO₂-ZnO nanocomposites is much weaker than C₆₀-ZnO and C₆₀-TiO₂ composites. According to TEM results, photocatalytic results show that C₆₀-TiO₂-ZnO nanocomposite have the highest percentage of dye degradation and the best photocatalytic properties due to having the best scattering.

How to cite this article

Mohamed W, Mohammed Z, Fadhil M. Synthesis, Characterization, Structural, Optical and Photocatalyst Properties of C₆₀-ZnO-TiO₂ Nano Hybrid. J Nanostruct, 2024; 14(1):93-100. DOI: 10.22052/JNS.2024.01.009

INTRODUCTION

One of the carbon allotropes is called fullerene, which is at nanoscale [1-2]. With the development of nanotechnology and nanoengineering, fullerene has played an important role in nano applications. Fullerenes are composed of graphite (graphene) layers with the difference that in their atomic structure, in addition to regularly arranged hexagons, there are pentagons that causes the plate not to be regular. These hexagons and pentagons together to allow the surface to be sphere, oval or cylinder is formed. The most common fullerene is called carbon 60, which contains 60 carbon atoms

[3]. The structure is the most spherical molecule known to man, that is firstly discovered in the laboratory in 1985 [4]. It has been found in natural environments such as rock [5], on the earth and in space [6]. In the structure of carbon 60, each carbon atom has a covalent bond with 3 adjacent carbon atoms. Carbon 60 is a molecule made of one element and in the form of a hollow cage. This property and the possibility of filling it, makes it a suitable option for building the drug delivery systems and antioxidants. The diameter of spherical fullerene is about 1nm. It is harder than

* Corresponding Author Email: anfal.fadhil@yahoo.com



diamond (its hardness is more than diamond) and has promising applications as a polymeric filler to increase mechanical strength [7].

Weather (climate) pollution is one of the main problems of environment around the world, hence, in the last decade, restoring the environment and eliminating the pollution has been one of the global priorities. One way to eliminate the pollutions is to use nanophotocatalysts. Among the photocatalytic materials used to eliminate the organic and inorganic pollutants, we can refer to ZnO, Fe₂O₃, WO₃, MoS₂, TiO₂ and CdS [8-15]. Among the well-known photocatalysts, titanium oxide and zinc oxide are of great interest to researchers. Therefore, in the research, we intend to investigate the photocatalytic properties of C₆₀/TiO₂, C₆₀/TiO₂/ZnO, C₆₀/ZnO nanocomposites.

MATERIALS AND METHODS

We mix fullerene (C₆₀) with water and place

in ultrasonic for 15 minutes until it is completely dispersed. We divide the obtained solution into three parts and 0.17g of zinc oxide nanopowder was added to one of the solutions, 0.17g of anatase titanium oxide nanopowder was added to the second solution, and 0.17g of zinc oxide nanopowder along with 0.17g of anatase titanium oxide nanopowder was added to the third solution. The mass ratio of fullerene to each of the nanoparticles of 20:1 was selected. The resulting solutions were dispersed in an ultrasonic bath for 1.5 h at 80°C. Each solution was then stirred in a water bath at 80°C. The powder obtained in the oven was dried at 100°C for 1.5 h.

RESULTS AND DISCUSSION

X-ray diffraction spectrum of C₆₀-ZnO, C₆₀-TiO₂ and C₆₀-TiO₂-ZnO samples were prepared to determine the crystallographic structure of the studied nanopowders. X-ray diffraction (XRD)

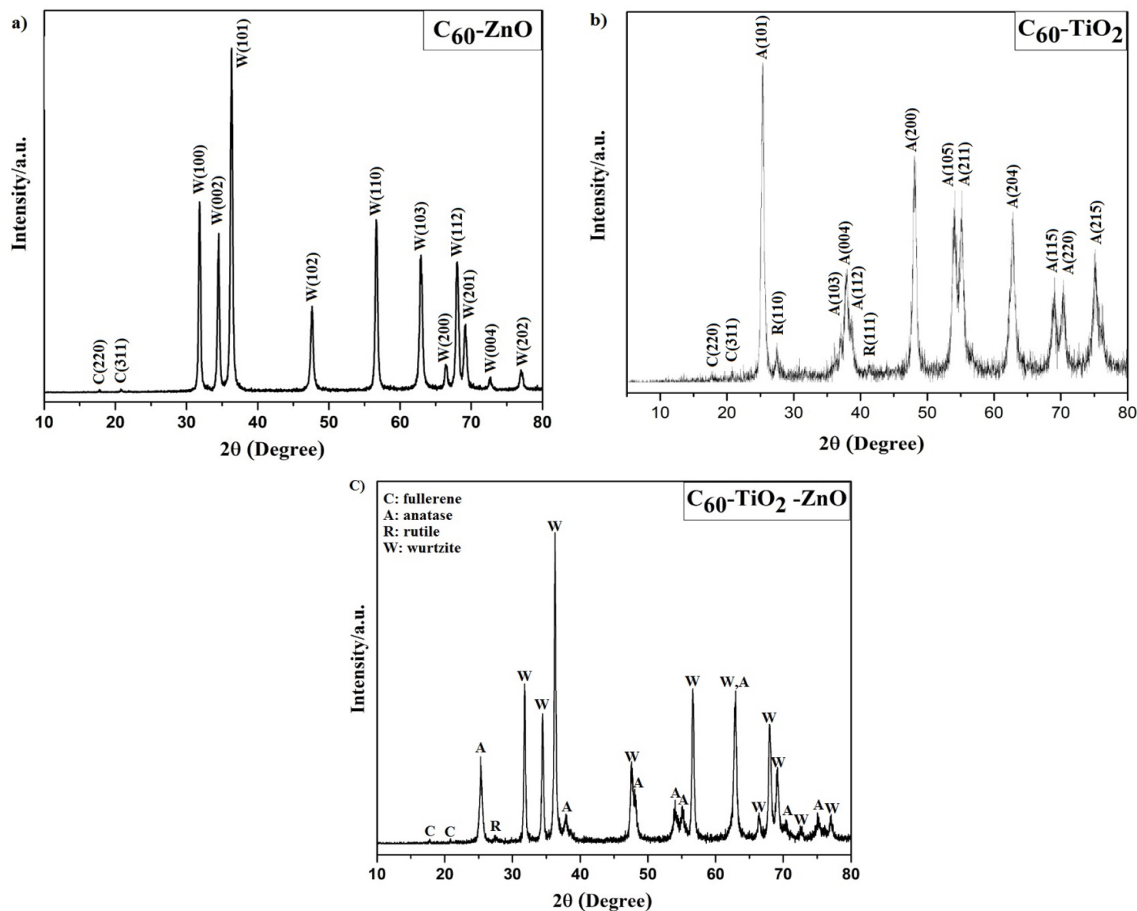


Fig. 1. XRD Diagram of Nanopowders of a) C₆₀-ZnO, b) C₆₀-TiO₂ and c) C₆₀-TiO₂-ZnO.

spectrum were measured using D8 Advance Bruker YT and CuK α radiation with the wavelength of $\lambda=1.5418\text{\AA}$ at 2θ values between 10° and 80° . XRD diagram of C₆₀-ZnO, C₆₀-TiO₂, and C₆₀-TiO₂-ZnO samples are plotted in Fig. 1a, b, and c, respectively. According to Fig. 1, the peak related

to fullerene is observed in all samples at angles of $2\theta=17.8, 20.8^\circ$, which are related to planes of (111), (220), respectively. Similar results have been reported by other researchers [16-17]. Fullerene peak is marked with the symbol C in Fig. 1. In Fig. 1a, the peaks located at angles of $2\theta=31.83$

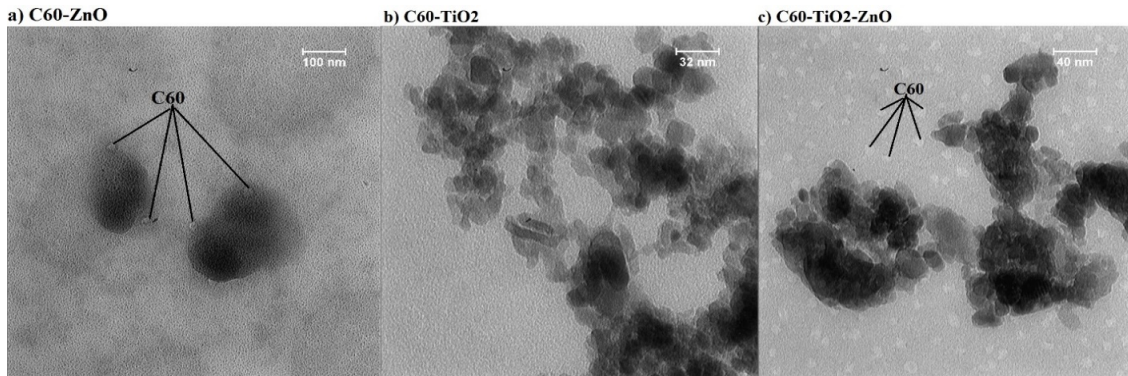


Fig. 2. Transmission Electron Microscope (TEM) Images of Nanopowders of a) C₆₀-ZnO, b) C₆₀-TiO₂ and c) C₆₀-TiO₂-ZnO

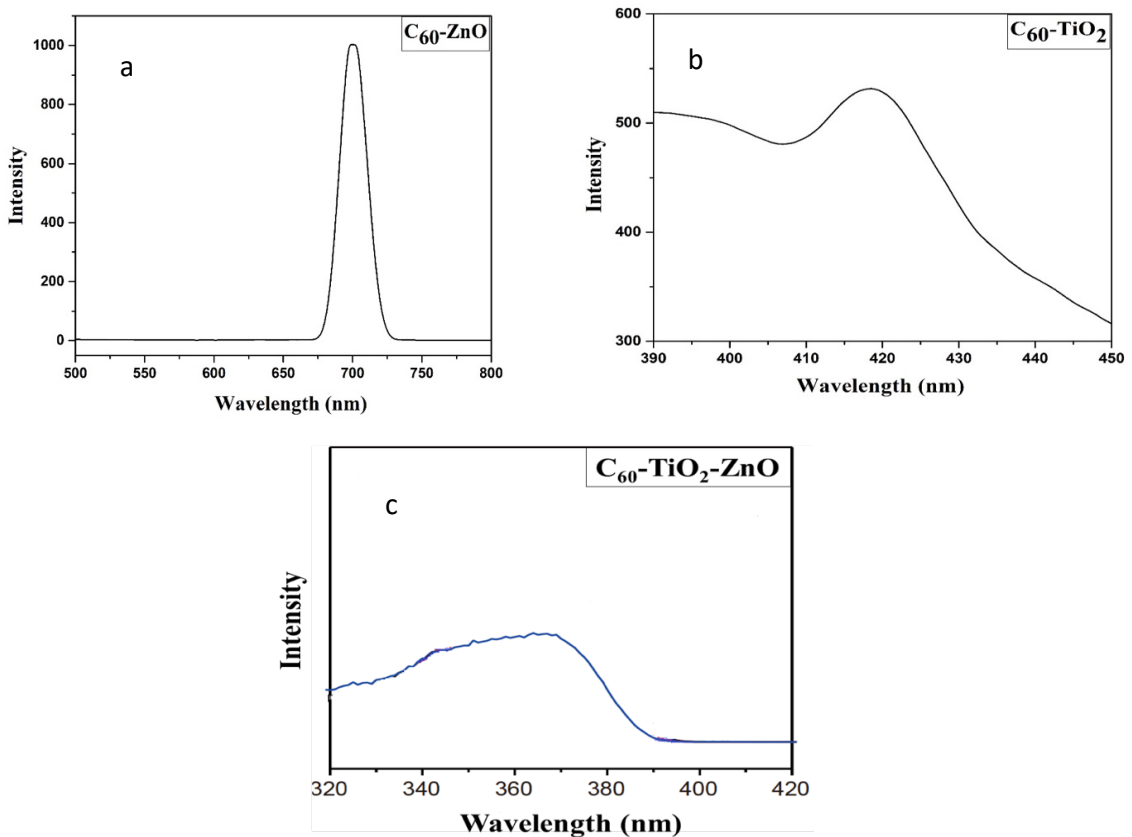


Fig. 3. a) photoluminescence (PL) spectrum of C₆₀-ZnO nanocomposite b) photoluminescence (PL) spectrum of C₆₀-TiO₂ nanocomposite c) photoluminescence (PL) spectrum of C₆₀-TiO₂-ZnO nanocomposite

(100), 34.48 (002), 36.31 (101), 47.62 (102), 56.66 (110), 62.92 (103), 66.42 (200), 66.56 (112), 68.00 (201), 73.90 (004), 77.18 (202) correspond to JCPDS, NO. 36-1451 which is related to wurtzite hexagonal structure of zinc oxide [16-17]. Zinc oxide has a spatial group P 63 m c and its lattice constants are $a = 3.2494 \text{ \AA}$ and $c = 5.2038 \text{ \AA}$ and no additional peak is observed in the structure. The peak related to zinc oxide is marked with the symbol W in Fig. 1. Fig. 1b shows peaks related to both anatase and rutile phases, although 84.9% of the peaks are related to anatase phase and only 15.1% are related to rutile phase. Anatase phase is marked with the symbol A and rutile phase with the symbol R. Titanium dioxide has a tetragonal crystal structure in which Anatase phase has the spatial group I 41/a m d and rutile phase has the spatial group P 42/m n m. Lattice constants of anatase phase of $a = 3.7850 \text{ \AA}$ and $c = 9.5140 \text{ \AA}$ and lattice constants of rutile phase of $a = 4.5937 \text{ \AA}$ and $c = 2.9581 \text{ \AA}$ were obtained. The peaks related to anatase phase are located at angles of $2\theta = 25.34 (101), 37.02 (103), 37.90 (004), 38.61 (112), 48.10 (200), 54.07 (105), 55.12 (211), 62.78 (204), 69.03 (115), 70.35 (220), 74.08 (215)$ that are consistent with PDF#21-1272 [18-19]. The peaks related to rutile phase are located at angles of $27.47^\circ, 41.29^\circ$, which are related to planes (110) and (111), respectively. Fig. 1C shows all peaks related to fullerene (C), wurtzite (W) phase of zinc oxide, anatase (A), and rutile (R) phases of titanium dioxide, exactly the same as C₆₀-ZnO and C₆₀-TiO₂ single composites.

In order to determine the morphology of the synthesized nanopowders, transmission electron microscope image was prepared from all samples. TEM images of the samples are reported in Fig. 2 for the nanopowders of a) C₆₀-ZnO, b) C₆₀-TiO₂ and c) C₆₀-TiO₂-ZnO. According to Fig. 2, it is clear that fullerene nanoparticles have a spherical shape, the size of fullerene nanoparticles is very small and less than 10nm. Fullerene nanoparticles are located outside the surface of zinc oxide and titanium dioxide nanoparticles. Titanium nanoparticles are less than 30 nm and zinc oxide nanoparticles are less than 50 nm in size and have the good scattering. Fullerene nanoparticles in C₆₀-TiO₂-ZnO sample show the best scattering and are not agglomerated. In C₆₀-ZnO sample, fullerene scattering is relatively good, but in C₆₀-TiO₂ sample, fullerene nanoparticles are not clearly specified (visible). Compared to agglomerated particles,

good dispersion of small particles can create more active sites for reaction. Similar images of fullerene nanocomposites with TiO₂ and ZnO have been reported by researchers [20-23].

In order to study the optical properties of C₆₀-ZnO, C₆₀-TiO₂ and C₆₀-TiO₂-ZnO composite powders, photoluminescence (PL) spectrum is shown in Fig.s 3a, b and c.

The photoluminescence spectrum of C₆₀-ZnO composite shown in Fig. 3a only shows a strong and broad emission band with a center of $\sim 700 \text{ nm}$, this emission is usually related to point defects such as: oxygen vacancy, zinc vacancy, interstitial oxygen, interstitial zinc, hydroxyl group and so on [24-28]. Typically, ZnO shows two emission bands: one in UV domain due to the band-edge emission and the other in the visible region due to the defect emission [26]. In this case, the explanation for the uncertain identification of UV emission considers a neutral peak resulting from the high density of point defect in ZnO.

In order to clarify the exact trend of charge carrier separation and recombination in the measurement of C₆₀-TiO₂ nanocomposite, photoluminescence (PL) spectrum measurement was systematically performed [29]. Upon UV excitation at 300 nm, the steady-state PL spectrum was recorded for C₆₀-TiO₂ in the range of 390-450 nm (Fig. 3b), in which a prominent peak of about 420 nm is attributed to TiO₂ bandwidth transmission [30]. It is obvious that PL emission of C₆₀-TiO₂-ZnO nanocomposite is much weaker than C₆₀-ZnO and C₆₀-TiO₂ composites (Fig. 3c). There are two main reasons for the decrease in PL spectrum intensity in triple nanocomposite. On the one hand, C₆₀ component from which the electron exits acts as an excellent receiver for electrons produced by light in TiO₂ conduction band, thus inhibiting the charge-carrier recombination trend observed in C₆₀-TiO₂ hybrid [31-33].

FTIR spectrum of C₆₀-ZnO nanocomposite is shown in Fig. 4a. The broad peak of about 3500 cm^{-1} is absorbed due to water molecules. The two peaks at 1554 cm^{-1} and 1415 cm^{-1} can be attributed to C-C elongation, while the bands observed at 840 cm^{-1} can be assigned to C-H functional groups. The characteristic band of Zn-O bond, which allows us to confirm the presence of zinc oxide, is located at 1618 cm^{-1} [34].

FT-IR measurement was performed to further elucidate the chemical composition of C₆₀-TiO₂ nanocomposite and can be seen in Fig. 4b. The

bands seen in the range of 500-1000 cm⁻¹ are attributed to the tensile vibration of Ti-O-Ti bonds (505 cm⁻¹) and Ti-O bonds (712 and 889 cm⁻¹). It should be noted that these bands have a high displacement compared to TiO₂ nanoparticles due to the significant interaction between TiO₂ and C₆₀.

In the case of C₆₀-TiO₂-ZnO triple nanocomposites (Fig. 4c), FT-IR spectrum shows the detectable peaks in 1093, 1382, and 1527 cm⁻¹ that are originated from C₆₀-ZnO. It should be noted that FT-IR spectrum in C₆₀-ZnO and C₆₀-TiO₂ composites shows a peak close to 1700 cm⁻¹, which is attributed to the asymmetric tensile vibration of carbonyl group in carboxylic acid, which is unexpectedly disappeared in triple composites [35].

200 ml of 1ppm methylene blue solution was prepared for each sample. 0.05g of C₆₀-ZnO, C₆₀-TiO₂ and C₆₀-TiO₂-ZnO nanopowders were added

to each solution. The solutions were stirred in the dark for 30 minutes until the adsorption-desorption operation is performed and the samples reach the equilibrium. We separate 5 ml of these solutions for UV-Vis test (A₀). The solutions were then irradiated for 120 minutes with UVC (200-280 nm) and UVB (280-315 nm) lamps each with the power of 18W. After 120 minutes, 5 ml of solution was taken from each sample for UV-Vis test (A_t). The percentage of methylene blue degradation is calculated using the relation A₀-A_t/A₀ [36]. The absorption spectrum of the samples in terms of wavelengths at zero and 120 minutes are plotted in Fig. 5.

According to Fig. 5, it is clear that after 120 minutes, a noticeable decrease is observed in the absorption spectrum of the samples. The percentage of methylene blue degradation at the wavelength of 663nm for C₆₀-ZnO, C₆₀-TiO₂ and

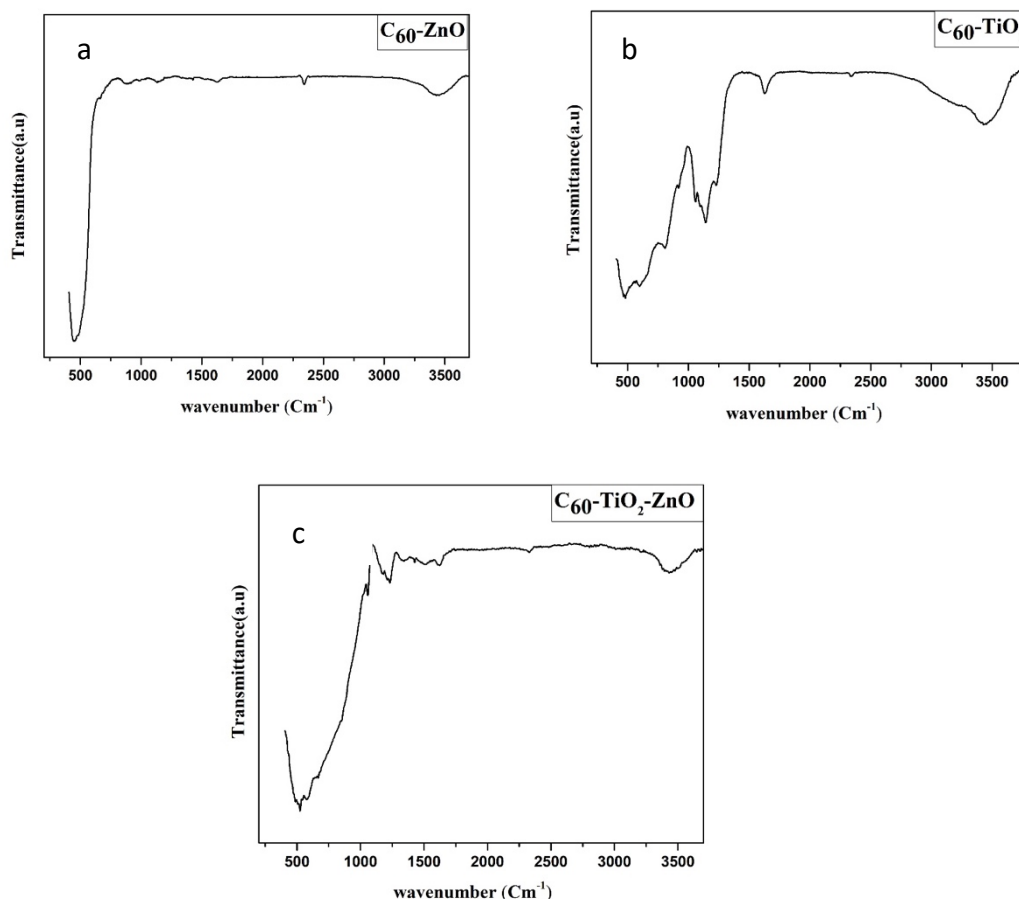


Fig. 4. a) FTIR spectra C₆₀-ZnO nanocomposites b) FTIR spectra C₆₀-TiO₂ nanocomposites c) FTIR spectra C₆₀-TiO₂-ZnO nanocomposites

C₆₀-TiO₂-ZnO nanopowders is 64.21%, 26.23% and 70.77%, respectively. C₆₀-TiO₂-ZnO nanocomposite has the highest percentage of dye degradation and the best photocatalytic properties. As

mentioned in the discussion of TEM images, fullerene nanoparticles have the best scattering in C₆₀-TiO₂-ZnO sample, and fullerene nanoparticles have the best scattering in C₆₀-TiO₂-ZnO sample,

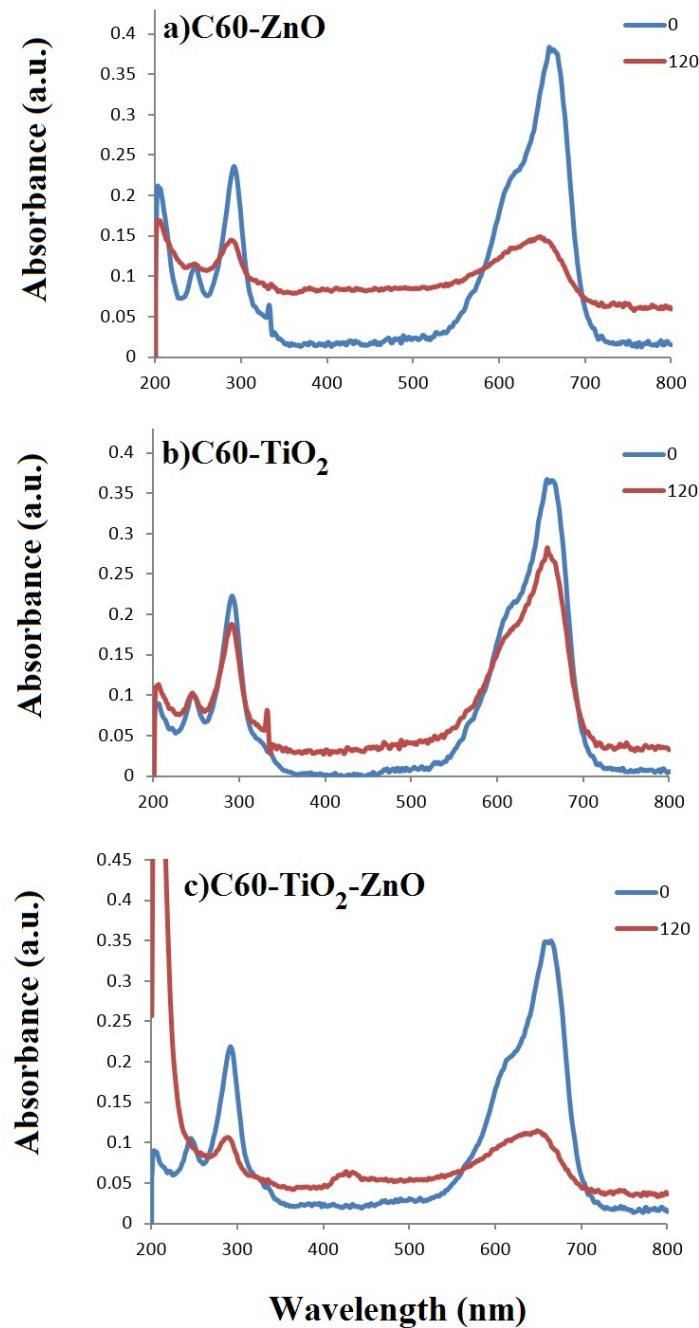


Fig. 5. Absorption Spectrum of Samples in Terms of Wavelength at Zero and 120 Minutes, a) C₆₀-ZnO, b) C₆₀-TiO₂ and c) C₆₀-TiO₂-ZnO

in C₆₀-ZnO nanocomposite, the scattering is also relatively good, but in C₆₀-TiO₂ sample, fullerene nanoparticles are not clearly visible. Therefore, C₆₀-TiO₂-ZnO nanocomposites, which have the best scattering of fullerene and whose particles are not agglomerated, show the highest percentage of dye degradation, and good dispersion of small fullerene nanoparticles can provide more active sites for better photocatalytic activity. However, in C₆₀-TiO₂ sample, where fullerene particles are not clearly specified, the lowest percentage of methylene blue degradation is observed. Therefore, it can be concluded that the higher the particle scattering and the lower the agglomeration rate, it shows the better photocatalytic properties.

Cho et al [16] have synthesized the Nanowhisker-ZnO (C₆₀) nanocomposites and studied the dye degradation of methylene blue using this nanocomposite. Their results show that various factors such as particle size and surface porosity affect the photocatalytic properties. Photocatalytic properties are improved by reducing the particle size and increasing the surface porosity. Pan et al [36] have studied the photocatalytic activity of a set of anatase samples with the dominant faces of {001}, {101} and {010}, in the presence and absence of fullerene. Based on their results, all samples show very similar activity in the presence of fullerene, while after removal of fullerene, the sample with the highest percentage {010} has the best photocatalytic activity, while the sample with the lowest percentage {001} shows the worst result. The effect of fullerene addition on the photocatalytic properties of anatase titanium dioxide has been studied by Bellardita et al [19]. When the reaction mechanism requires OH-radical intervention, the addition of C₆₀ has a positive effect on photocatalytic properties, as the researchers said. However, when the reaction is carried out by photogenerated holes, the addition of fullerene can have a negative effect on the dye degradation of methylene blue.

CONCLUSION

C₆₀-TiO₂, C₆₀-ZnO, C₆₀-TiO₂-ZnO nanocomposites were synthesized using sol-gel method. Structural results in C₆₀-ZnO samples show the wurtzite hexagonal structure of zinc oxide, in addition to the fullerene peak. In the sample of C₆₀-TiO₂ composite, the peaks related to both anatase and rutile phases are observed.

All peaks related to fullerene (C), wurtzite

(W) phase of zinc oxide and anatase (A) and rutile (R) phases of titanium dioxide are also exactly the same as C₆₀-ZnO and C₆₀-TiO₂ single composites in XRD analysis results of C₆₀-TiO₂-ZnO nanocomposites. The results of TEM images show that fullerene nanoparticles are located outside the surface of zinc oxide and titanium dioxide nanoparticles. Titanium nanoparticles are less than 30nm and zinc oxide nanoparticles are less than 50nm in size. Fullerene nanoparticles in C₆₀-TiO₂-ZnO sample show the best scattering and are not agglomerated. In C₆₀-ZnO sample, fullerene scattering is relatively good, but in C₆₀-TiO₂ sample, fullerene nanoparticles are not clearly specified. The photoluminescence (PL) spectrum measured for C₆₀-TiO₂-ZnO nanocomposite is much weaker than C₆₀-ZnO and C₆₀-TiO₂ composites. According to TEM results, photocatalytic results show that C₆₀-TiO₂-ZnO nanocomposite have the highest percentage of dye degradation and the best photocatalytic properties, due to having the best scattering.

CONFLICT OF INTEREST

The authors declare that there is no conflict of interests regarding the publication of this manuscript.

REFERENCES

1. Carbon Molecules and Materials: CRC Press; 2002 2002/04/11.
2. Henini M. Properties of Lattice-matched and Strained Indium Gallium Arsenide by P. Bhattacharya (Ed.). London: INSPEC, the Institution of Electrical Engineers, ISBN 0-85296-865-5; Properties of Indium Phosphide, London: INSPEC, the Institution of Electrical Engineers, ISBN 0-85296-491-9; Properties of Aluminium Gallium Arsenide by S. Adachi (Ed.). London: INSPEC, the Institution of Electrical Engineers, ISBN 0-85296-558-3. Microelectron J. 1999;30(12):1273-1274.
3. Kohara H, Ishibashi N, Fujita S. Extraction of aliphatic monocarboxylic acids with high molecular weight amine. Bunseki Kagaku. 1968;17(7):854-863.
4. Kroto HW, Heath JR, O'Brien SC, Curl RF, Smalley RE. C60: Buckminsterfullerene. Nature. 1985;318(6042):162-163.
5. Buseck PR, Tshipursky SJ, Hettich R. Fullerenes from the Geological Environment. Science. 1992;257(5067):215-217.
6. Cami J, Bernard-Salas J, Peeters E, Malek SE. Detection of C₆₀ and C₇₀ in a Young Planetary Nebula. Science. 2010;329(5996):1180-1182.
7. Perspectives of Fullerene Nanotechnology. Kluwer Academic Publishers; 2002.
8. Levy B. J Electroceram. 1997;1(3):239-272.
9. Davis B. Encyclopedia of special education Cecil R. Reynolds and Lester Mann (Eds.). New York: John Wiley & Sons, 1987. 1793 pp., \$250.00. Arch Clin Neuropsychol. 1989;4(1):95-99.

10. Mills G, Hoffmann MR. Photocatalytic degradation of pentachlorophenol on titanium dioxide particles: identification of intermediates and mechanism of reaction. *Environmental Science & Technology*. 1993;27(8):1681-1689.
11. Karakitsou KE, Verykios XE. Effects of alervalent cation doping of titania on its performance as a photocatalyst for water cleavage. *The Journal of Physical Chemistry*. 1993;97(6):1184-1189.
12. Nair M, Luo Z, Heller A. Rates of photocatalytic oxidation of crude oil on salt water on buoyant, cenosphere-attached titanium dioxide. *Industrial & Engineering Chemistry Research*. 1993;32(10):2318-2323.
13. Front cover. *Photochem Photobiol Sci*. 2014;13(11):1489-1490.
14. Liao DL, Liao BQ. Shape, size and photocatalytic activity control of TiO₂ nanoparticles with surfactants. *J Photochem Photobiol A: Chem*. 2007;187(2-3):363-369.
15. Photocatalytic purification and treatment of water and air: Proceedings of the 1st International conference on TiO₂ photocatalytic purification and treatment of water and air, London, ON, Canada, 8–13 November 1992 Edited by D. Ollis, North Carolina State University, Raleigh, NC, USA and H. Al-Ekabi, Nutech Environmental, London, ON, Canada Trace Metals in the Environment Volume 3 (Elsevier Science Publishers, Amsterdam, 1993), ISBN 0-444-89855-7; 820 pages; price: Dfl. 450.00 (US \$257.25). *Sol Energy Mater Sol Cells*. 1994;32(2):220-220.
16. Cho BH, Lee KB, Miyazawa Ki, Ko WB. Preparation of Fullerene (C60) Nanowhisker-ZnO Nanocomposites by Heat Treatment and Photocatalytic Degradation of Methylene Blue. *Asian J Chem*. 2013;25(14):8027-8030.
17. Li P, Liu Y, Liu J, Li Z, Wu G, Wu M. Facile synthesis of ZnO/mesoporous carbon nanocomposites as high-performance anode for lithium-ion battery. *Chem Eng J*. 2015;271:173-179.
18. Zhou YQ, Wu BS, Lin GH, Xing Z, Li SH, Deng LL, et al. Interfacing Pristine C₆₀ onto TiO₂ for Viable Flexibility in Perovskite Solar Cells by a Low-Temperature All-Solution Process. *Advanced Energy Materials*. 2018;8(20).
19. Bellardita M, Garlisi C, Venezia AM, Palmisano G, Palmisano L. Influence of fluorine on the synthesis of anatase TiO₂ for photocatalytic partial oxidation: are exposed facets the main actors? *Catalysis Science & Technology*. 2018;8(6):1606-1620.
20. Meng Z-D, Zhu L, Choi J-G, Park C-Y, Oh W-C. Preparation, characterization and photocatalytic behavior of WO₃-fullerene/TiO₂ catalysts under visible light. *Nanoscale research letters*. 2011;6(1):459-459.
21. Cid A, Moldes ÓA, Diniz MS, Rodríguez-González B, Mejuto JC. Redispersion and Self-Assembly of C₆₀ Fullerene in Water and Toluene. *ACS omega*. 2017;2(5):2368-2373.
22. Meng Z-D, Zhu L, Choi J-G, Chen M-L, Oh W-C. Effect of Pt treated fullerene/TiO₂ on the photocatalytic degradation of MO under visible light. *J Mater Chem*. 2011;21(21):7596.
23. Zhang X, Wang Q, Zou L-H, You J-W. Facile fabrication of titanium dioxide/fullerene nanocomposite and its enhanced visible photocatalytic activity. *Journal of Colloid and Interface Science*. 2016;466:56-61.
24. Florica C, Preda N, Enculescu M, Zgura I, Socol M, Enculescu I. Superhydrophobic ZnO networks with high water adhesion. *Nanoscale research letters*. 2014;9(1):385-385.
25. Florica C, Costas A, Kuncser A, Preda N, Enculescu I. High performance FETs based on ZnO nanowires synthesized by low cost methods. *Nanotechnology*. 2016;27(47):475303.
26. Djurišić AB, Leung YH. Optical Properties of ZnO Nanostructures. *Small*. 2006;2(8-9):944-961.
27. Reshchikov MA, Morkoç H, Nemeth B, Nause J, Xie J, Hertog B, Osinsky A. Luminescence properties of defects in ZnO. *Physica B: Condensed Matter*. 2007;401-402:358-361.
28. Tam KH, Cheung CK, Leung YH, Djurišić AB, Ling CC, Belling CD, et al. Defects in ZnO Nanorods Prepared by a Hydrothermal Method. *The Journal of Physical Chemistry B*. 2006;110(42):20865-20871.
29. Hernández-Gordillo A, Romero AG, Tzompantzi F, Gómez R. Kinetic study of the 4-Nitrophenol photooxidation and photoreduction reactions using Cds. *Applied Catalysis B: Environmental*. 2014;144:507-513.
30. Wang E, Yang W, Cao Y. Unique Surface Chemical Species on Indium Doped TiO₂ and Their Effect on the Visible Light Photocatalytic Activity. *The Journal of Physical Chemistry C*. 2009;113(49):20912-20917.
31. Long Y, Lu Y, Huang Y, Peng Y, Lu Y, Kang S-Z, Mu J. Effect of C₆₀ on the Photocatalytic Activity of TiO₂ Nanorods. *The Journal of Physical Chemistry C*. 2009;113(31):13899-13905.
32. Cho E-C, Ciou J-H, Zheng J-H, Pan J, Hsiao Y-S, Lee K-C, Huang J-H. Fullerene C₇₀ decorated TiO₂ nanowires for visible-light-responsive photocatalyst. *Appl Surf Sci*. 2015;355:536-546.
33. Yu J, Ma T, Liu G, Cheng B. Enhanced photocatalytic activity of bimodal mesoporous titania powders by C₆₀ modification. *Dalton Transactions*. 2011;40(25):6635.
34. Saikia I, Hazarika M, Tamuly C. Synthesis, characterization of bio-derived ZnO nanoparticles and its catalytic activity. *Mater Lett*. 2015;161:29-32.
35. Max J-J, Chapados C. Infrared Spectroscopy of Aqueous Carboxylic Acids: Comparison between Different Acids and Their Salts. *The Journal of Physical Chemistry A*. 2004;108(16):3324-3337.
36. Pan Y, Birdsey RA, Phillips OL, Jackson RB. The Structure, Distribution, and Biomass of the World's Forests. *Annu Rev Ecol Evol Syst*. 2013;44(1):593-622.